- Technical Paper -

FINITE ELEMENT ANALYSIS ON THE CONCRETE BREAKOUT CAPACITY OF HEADED REINFORCEMENT BAR EMBEDDED IN L-SHAPED BEAM-COLUMN JOINTS

Zev A. JAUHARI[*1], Tomoya MATSUI[*2]

ABSTRACT

A nonlinear finite element model is developed to analyze the concrete breakout strength of the headed reinforcement bar embedded in roof exterior beam-column joints under pullout loading. The three-dimensional FE models were established using FINAL software and validated against the experimental results of beam-column joint specimens found in the literature. The proposed FE models closely predicted the behavior of the beam-column joint specimens in terms of pullout load capacity, failure mechanism, crack pattern, and strain at the reinforcing bars.

Keywords: finite element analysis, headed bar, concrete breakout strength, beam-column joint.

1. INTRODUCTION

The failure of beam-column joints is the primary factor in building collapses resulting from seismic activity. It establishes the necessity for an engineering methodology to implement efficient and cost-effective strategies to enhance joint performance [1]. Innovative joint designs that can reduce reinforcement congestion in the joint are desirable. The overlapping of the main and bending reinforcement bars results in congestion within the beam-column joint reinforcement configuration, adversely impacting the quality of concrete placement at the joint [2]. Using headed bars at the end of the reinforcement markedly decreases the anchorage length and addresses interweaving complications, facilitating improved concrete placement [3]. A headed bar offers an effective solution for reinforcement congestion. It is an alternative to hook termination and straight bars, reducing embedment lengths and simplifying design detailing [4].

Several studies have investigated the anchorage capacity of headed bars in concrete structural elements. An experimental study of pullout tests on the concrete breakout strength of headed reinforcement bars in L-shape beam-column joints has been conducted [5]. These experiments examined the concrete breakout strength of headed reinforcing bars under diverse conditions and yielded significant results that confirm and enhance current normative calculation models. Nevertheless, the intricate method of transmitting pullout loads through the beam-column joint in a concrete structure necessitates more advancements in regulatory standards to develop sufficient calculation criteria, mainly when supplementary bars are present. Creating a suitable numerical model may analyze the impact of various parameters on an innovative design. This is particularly applicable when interior crack propagation and stress concentrations are challenging to detect experimentally, as observed in reinforced concrete specimens. The finite element (FE) analysis method can present an accurate and cost-effective solution. This study performs FE analysis on the pullout experiment of mechanically anchorage rebar by Mohsuni et al. [5] to investigate the concrete breakout capacity of headed bars embedded in concrete elements on roof exterior beam-column joints under tensile loads. Therefore, a correlative study based on test specimens' pullout load and mechanical failure was conducted to verify the analytical model with the experimental results.

2. EXPERIMENTAL PROGRAMS

The prior study [5] performed pullout tests on 70% of full-scale beam-column joints to examine the anchorage capacity of headed bars, considering various parameters such as the diameter of the headed and hoops bars, including supplementary and intermediate reinforcing bars. Four typical specimens were experimentally analyzed to determine their pullout forces: LE25-M, LE25-Ma, LC25-M, and LC25-Mb. Fig. 1 illustrates a standard cross-section of LE25-M and LC25-Mb specimens incorporating headed bars. LE25-M served as the benchmark specimen, with the headed bars functioning as the primary bars of the column across all specimens. Subscripts "a" and "b" were employed for these two specimens to differentiate them from the benchmark specimen. Specimen LE25-Ma differed from LE25-M just in the diameter of the supplementary bar; specimen LE25-Ma was 6 mm, while LE25-M utilized a diameter of 13 mm. The experiment also utilized specimens featuring single-headed bars (LC25-M and LC25-Mb). LC25-Mb had three layers of supplementary

*1 Graduate School of Engineering, Toyohashi University of Technology, JCI Member
*2 Associate Prof., Dept. of Civil Engineering, Toyohashi University of Technology, Dr. E., JCI Member

and intermediate bars, whereas model LC25-M had supplementary bars only. All specimens were designed to show concrete cone or side blowout failure. Tables 1 and 2 list the material properties of the concrete and steel reinforcing bars based on the compression, splitting, and tensile tests, respectively. Fig. 2 illustrates the loading mechanism used in the experiment, wherein the force application beam receives the reaction force, and a central hole jack directly tensions each headed bar.

Table 1 Material properties of concrete

Specimen	Compressive strength σ_B (N/mm^2)	Tensile strength f_t (N/mm^2)	Elastic modulus E_c (N/mm^2)
LE25-M	33.2	2.8	27900
LE25-Ma	32.6	2.8	27800
LC25-M	33.2	3.2	26900
LC-25Mb	34.4	2.8	28000

Table 2 Material properties of reinforcing bars

Material type	Yield stress σ_y (N/mm^2)	Young modulus E_s (N/mm^2)	Remark
D6 (SD295)	407	195000	Supplementary bar
D13 (SD295)	342	193000	Sup. / Int. bar
D25 (SD390)	441	196000	Beam main bar
D25 (USD980)	1095	194000	Headed bar

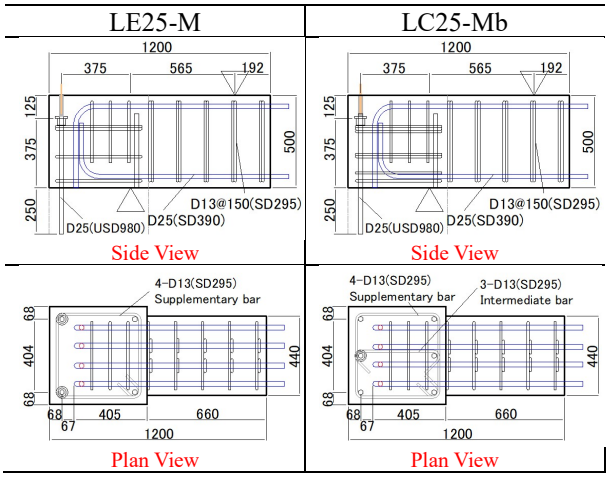

Fig.1 Cross-section and detail of the LE25-M and LC25-Mb Specimens (unit: mm)

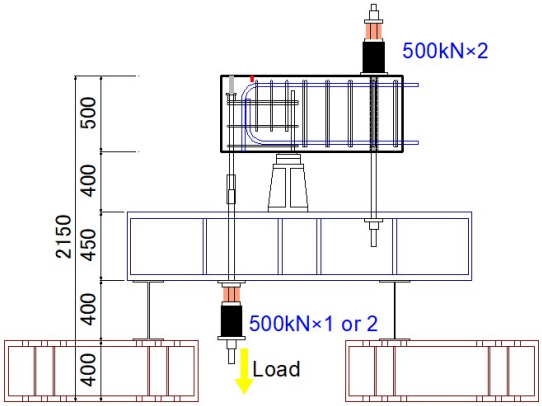

Fig.2 Schematic illustration of test setup

The pullout loads of the headed bars were measured using load cells positioned at the top of the jacks. Displacement transducers were affixed to the plate nut's upper side to measure the headed bars' withdrawal displacement. The anchorage capacity of the headed bars was substantially impacted by supplementary bars, as indicated by the test results. The supplementary bars augmented the concrete's diagonal force to withstand the applied pullout load. Consequently, an adequate number of supplementary bars must be used.

3. NUMERICAL MODEL

3.1 Elements Used

The non-linear FE analysis used FINAL v11 [6] software to model the beam-to-column joint specimens. The details of the beam-column joints model are shown in Fig. 3. The analysis was performed in three dimensions, and a triaxial stress field was assumed. Concrete was designed as 8-node hexahedral elements, and reinforcing bars were replaced using a 1D line element (beam element). The headed bars in the FEA model are modeled using a 4-node quadrilateral. The slippage between the main-headed reinforcing bars and concrete was modeled by inserting the 4-node line element. This element provides contact points for the concrete and reinforcing bar elements, which are defined separately. To model the interface between the plate nut and concrete, the nodes on the top plate nut are not connected to the concrete nodes on the plate nut (separate nodes), while the bottom is directly connected to the concrete nodes under the plate nut (same nodes).

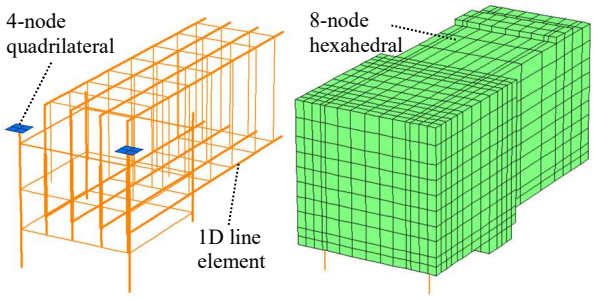

Fig.3 The 3D model of the beam-column joint specimen (LE25-M) developed in FINAL

3.2 Material Constitutive Model

The modified Ahmad model calculated the concrete compressive stress-strain relationship in the FE model [7]. Based on fracture energy, the Nakamura-Higai model [8] was used for the stress decrease region, as shown in Fig. 4. The model was designed so that only the area corresponding to the beam-column joint panel cover was brittle since the model was developed to break due to concrete failure only (cone or side blowout mode). The Ottosen four-parameter model is used for fracture conditions under triaxial stress. The crack-softened area on the tension side was assumed to bear almost no tensile stress after cracking, and strain reduction after cracking was not considered. The tension stiffening characteristic

by the Izumo et al. [9] model was used, and the coefficient C was set to 1.0, assuming that almost no tensile stress is borne after cracking. The shear transfer model after cracking on the beam was based on the Naganuma model [7], while the joint was assumed to have no shear transfer (zero shear stiffness). The factor of reducing compressive strength after cracking in the FE model uses Collins et al.'s [10] proposed formula. Since the LE25-Ma model has an unstable pullout capacity curve after reaching the peak pullout load due to the divergence of the solution, Naganuma's proposed formula was used [11]. However, using Naganuma's proposed formula in other models (LE25-Ma, LC25-M, and LC25-Mb) underestimates the anchorage capacity. The anchorage capacity for analytical results is much lower than the test. So, the setting for reducing the compressive strength factor of LE25-Ma is different from that of the other models.

The stress-strain relationship adopted to represent reinforcement bar behavior was the modified Menegotto-Pinto model. The anchor plate was modeled as perfect elastic bodies with Young's modulus of 2.05 x 10^5 N/mm^2. The bond characteristics between headed reinforcing bars and concrete were based on the model by Naganuma et al. [7], and the slip at the maximum bond stress was assumed to be 1.0 mm. Then, peak stress was calculated based on *fib* Model Code 2010 ($\tau_u = 2.5\sqrt{f_{cm}}$) [12]. Fig. 5 shows the bond stress and slip relationship between reinforcing bars and concrete. The bond between the transverse reinforcement and concrete is assumed to be perfectly bonded.

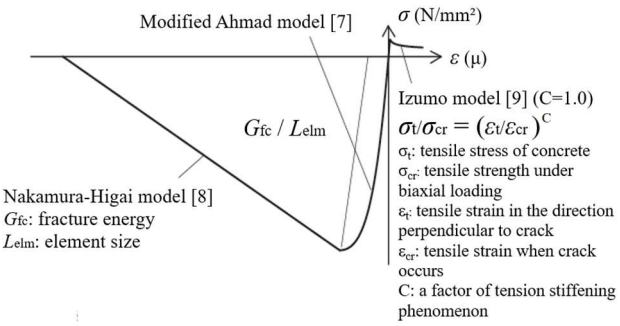

Fig.4 Principal stress equivalent uniaxial strain relation of concrete

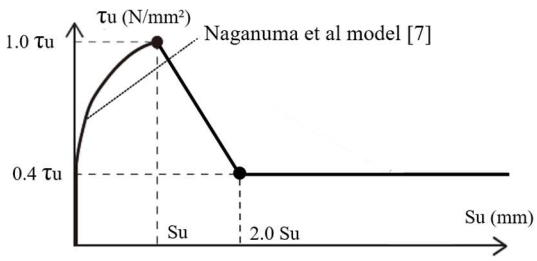

Fig.5 Bond stress-slip relationship

3.3 Loading and Boundary Condition

To simulate the test setup in the FEA model, boundary conditions must be applied to a specific plane in the model. In this analysis, the pin support on point A of Fig. 6 was restrained only in the z direction, and the support on point B was fixed in the x and z directions. The load is applied in a displacement-controlled mode in the downward direction at the lowest node of the headed reinforcement (point C) to reach a displacement of 50 mm, and the analysis was terminated when the specified step value was reached. Separate nodes were defined for the concrete and the anchor plate to reproduce the pull-out displacement at the anchor plate.

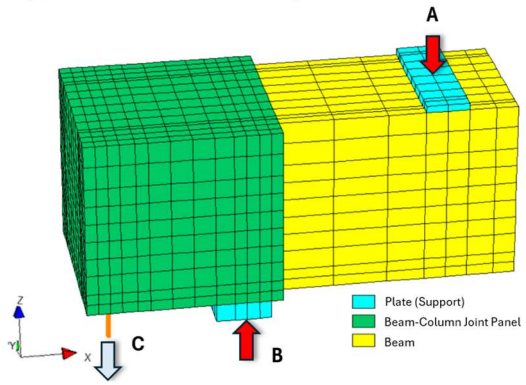

Fig.6 The 3D model of the beam-column joint specimen developed in FINAL

4. VALIDATION OF FE MODEL WITH TEST RESULTS

4.1 Pullout load vs displacement response

Figs. 7 and 8 compare the applied pullout load versus displacement curves predicted using the FE analysis and the experimental one of LE25-M, LE25-Ma, LC25-M, and LE25-Mb, respectively. The pullout displacement was calculated from the difference between the position of the displacement gauge installed during the experiment and the position of the anchorage bar, as shown in Fig. 9. Therefore, in the FE analysis, the displacement value (δ) was calculated by displacement on nodal A minus displacement on nodal B ($\delta = \delta_A - \delta_B$).

Fig. 7 shows an increase in strength after the pullout displacement progresses but generally shows a good correspondence on the model LE25-Ma. Model LE25-M showed a higher anchorage capacity than model LE25-Ma owing to its larger hoop diameter. Moreover, model LE25-M indicated increased pullout load despite its higher anchorage capacity after diagonal cracks appeared. Unlike model LE25-M, model LE25-Ma showed a lower anchorage capacity and a significant decrease in the pullout load after the emergence of diagonal cracks. Both FE models have excellent agreement between the numerical and experimental curves regarding initial stiffness and pullout load progress until displacement of 1.5 mm and 4 mm for LE25-M and LE25-Ma, respectively.

Fig. 8 compares the pullout load-displacement relationship of the models with and without intermediate supplementary bars. Both test and analysis results show that LC25-Mb exhibited a higher anchorage capacity than LC25-M. The presence of supplementary bars in the form of hoops or intermediate reinforcing bars significantly increased the anchorage capacity of the model.

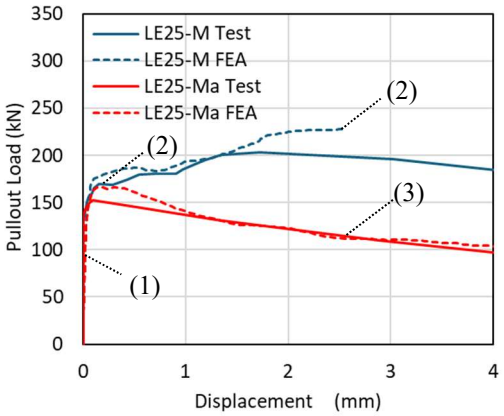

Fig.7 Pullout load-displacement relationship of LE25-M and LE25-Ma specimens

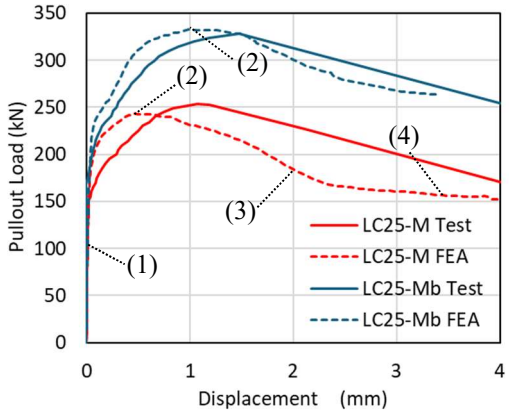

Fig.8 Pullout load-displacement relationship of LC25-M and LC25-Mb specimens

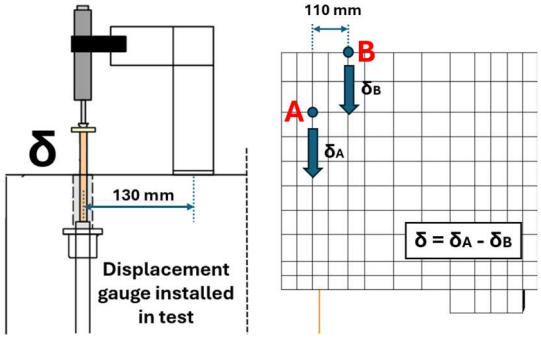

Fig.9 Pullout displacement calculated for test and FE analysis

4.2 Failure Mechanism (Crack Pattern)

Validation of the crack pattern on the concrete is necessary to verify the possibility of undesirable tensile load effects due to the rapid appearance of cracks in the concrete because of the headed bar pullout. Fig. 10 compares crack patterns on the concrete in LE25-Ma between the test and FE analysis. The number sign in Figs. 10 and 11 corresponded to Figs. 7 and 8, respectively. The failure mechanism in the test and FEA was as follows: (1) a vertical crack first emerged from the bottom of the beam-column joint region along the headed bar, and (2) as the load increased to reach the peak load, diagonal cracks began to appear around the anchorage bar. The development of diagonal cracks in the FE model is close to the test results. (3) Finally, further diagonal cracks appeared in the beam-column joint panel, and the pullout displacement of the anchorage bar began to occur. When diagonal cracks also appeared near the anchor plate, the pullout load of the anchorage bar began to decrease. FEA and test results show that cone cracking occurred in the cover concrete near the anchorage, resulting in ultimate failure. For the LE25-M model, the failure process is like the LE25-Ma model.

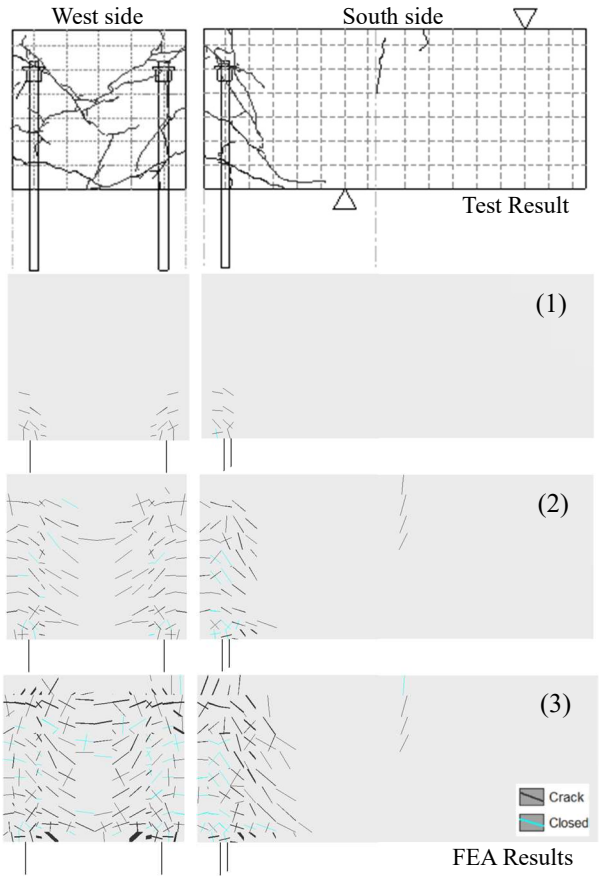

Fig.10 Crack patterns of LE25-Ma specimen and the FE model

Fig. 11 compares crack patterns on the concrete in LC25-M between test and FE analysis from the west and bottom side views. As seen from the west side, the failure state was: (1) vertical cracks emerged from the bottom of the joint region along the headed bar, located at the midpoint of the beam-column joint cross-section. (2) As the pullout load increased, diagonal cracks appeared at the bottom of the header bar in the beam-column joint region. In contrast, vertical cracks appeared along the headed bar extended toward the upper side. (3) As the pullout load increased, horizontal cracks appeared near the plate nut. (4) The pullout load decreased, and the cracks extended toward the left and right sides of the headed bar. From the bottom side, the crack pattern was as follows: (1) cracks emerged from the headed reinforcing bars at the midpoint of the beam-column joint cross-section. (2) As the pullout load increased, the crack extended toward the bar's left, right, and bottom. (3) The crack propagated into the column's main reinforcing bar. Although there were some differences in

the timing of crack occurrence between the experiment and analysis, the tendency of crack occurrence was generally reproduced well. Overall, the comparison of the concrete fracture process and pullout load-displacement response of the FE model generally showed good agreement with the experiment.

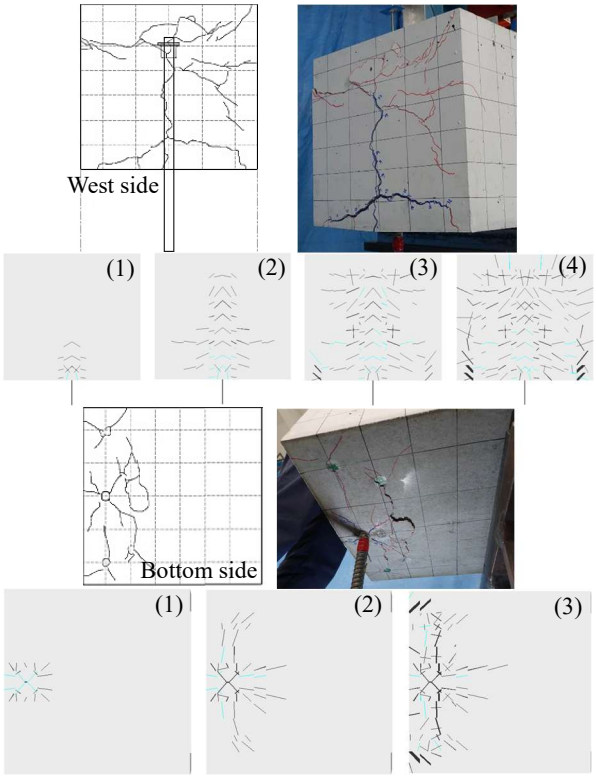

Fig.11 Crack patterns of LC25-M specimen and the FE model

4.3 Minimum Principal Stress and Strain of Reinforcing Bars

The analytical minimum principal stress of the FE analysis is compared with test results in Fig. 12 for LE25-M, LC25-M, and LC25-Mb, respectively. Fig. 13 shows a cutaway diagram showing the location of the tensile and supplementary rebars. The stress contour displayed in the figure occurs at the pullout load indicated as (2) in Fig. 7 and 8. Generally, the analytical first cracks are inclined and concentrated in the bottom of the headed reinforcing bar area, where the crack first occurs. Then, the stress acts in a 45-degree direction from the anchorage rebar. Due to stress concentration, cracks may initiate at the anchorage region of the headed bars. All FE models show that the stress was concentrated on the near plate nut at the maximum pullout load. The stress contour of LE25-M and LC25-M showed that the stress was concentrated in the first supplementary bar (from the top). On the LC25-Mb model, stress was concentrated in the top and middle intermediate supplementary bars, indicating that the presence of supplementary and intermediate bars is important to bearing the pullout load and increasing the concrete breakout capacity. All models displayed that the stress is not acting in the headed reinforcing bar area. These results allowed us to confirm the stress state at the time of fracture. The concentrated stress on the FE model could accurately predict the specimens' failure.

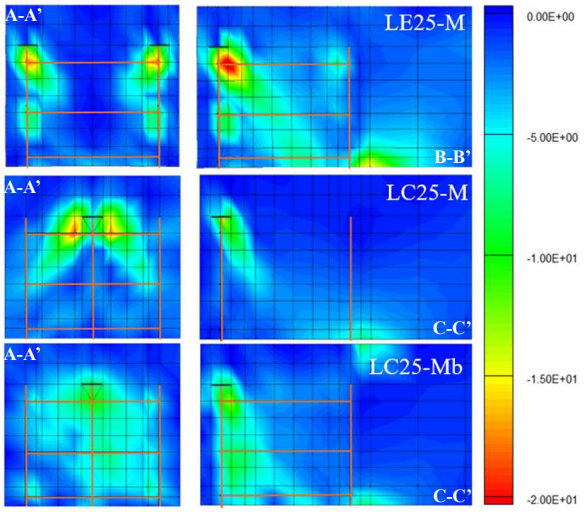

Fig.12 Minimum principal stress of LE25-M, LC25-M, and LC25-Mb model

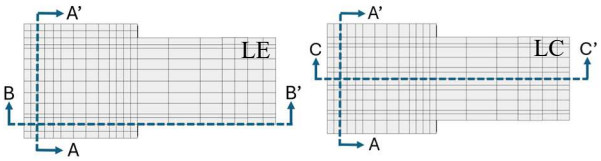

Fig.13 Cutaway of LE and LC models

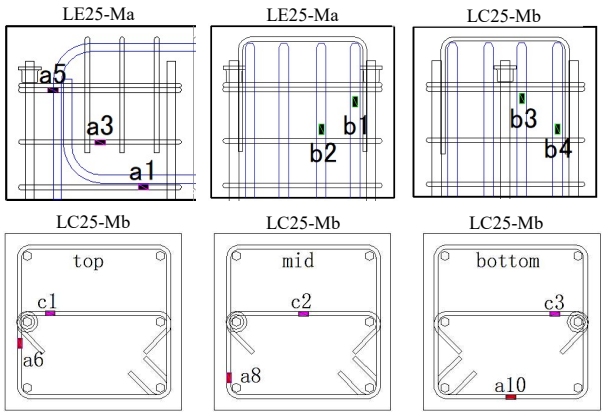

Fig.14 Location of strain gauges of LE25-Ma and LC25-Mb specimens

Fig. 14 illustrates the positions of the strain gauges in specimens where the strain was measured for comparison with FE analysis. Fig. 15 shows the pullout load and strain relationship on the supplementary and main beam bars of the LE25-Ma model. The supplementary bars show higher strain readings at a3 and a5 rather than test results. The strain at a1 indicates that the supplementary bar was compressed under pullout load. The strain at the main bar shows that b1 has a higher strain than b2. Fig. 16 compares the pullout load and strain relationship in LC25-Mb reinforcing bars. The strain at c1 (most top intermediate bars) is higher than that at other supplementary and intermediate bars. This clearly shows that the higher concrete breakout capacity affects an intermediate bar's presence, especially near the

plate nut. These findings validate the FE model's capability to simulate the experimentally observed strain at reinforcing bars. Therefore, the model is suitable for predicting the anchorage capacity of headed reinforcement bars embedded in concrete elements and can be used in future parametric studies.

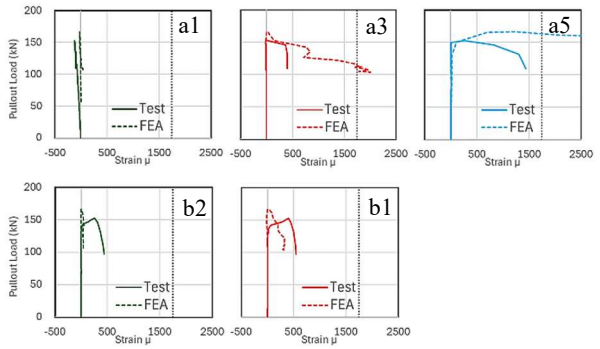

Fig.15 Relationship between load and strain of supplementary and main beam bars of LE25-Ma

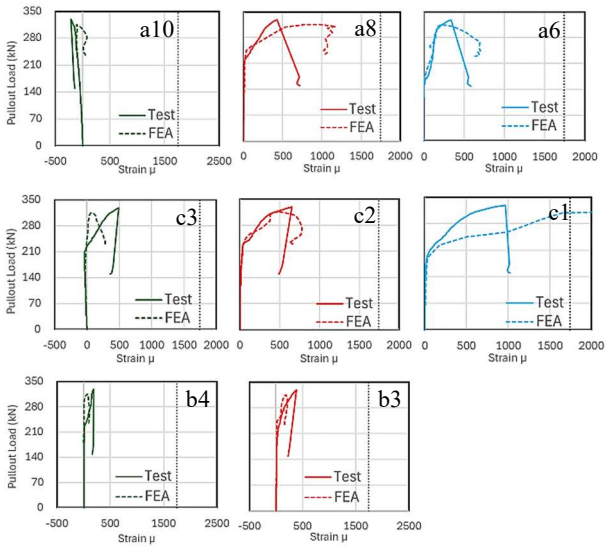

Fig.16 Relationship between load and strain of supplementary, intermediate, and main beam bars of LC25-Mb

5. CONCLUSIONS

(1) The non-linear FE model presented in this study accurately predicted the concrete breakout strength of the headed reinforcement bar for experimentally tested roof exterior beam-column joint specimens. Pullout load-displacement relationship, crack patterns, stress, and strain distribution results for theoretically studied specimens were simulated accurately using FINAL software.

(2) The anchorage capacity of the headed bars was substantially impacted by supplementary bars, as indicated by the test and FE analysis results. The supplementary bars augmented the concrete's diagonal force to withstand the applied pullout load.

(3) The diameter of supplementary bars significantly affected the anchorage capacity. Therefore, the FE parametric analysis can be performed in the following study to investigate the influence of diameter and number of supplementary bars.

REFERENCES

[1] Pawar, V.R., Patil, Y.D., and Patil, H.S., "Cyclic loading of Exterior Beam - Column Joint with Threaded Headed Reinforcement", Int. Journal of App. Eng. Research, Vol. 12, No. 17, pp. 6377-6383, 2017.

[2] Miao, T., Yang, J., Zhou, Y., Zhan, M., Sha, L., and Zheng, W., "Research on the Distributive Relationship between Bond Force and Bearing Pressure for Anchorage Force by Headed Bars", Buildings, Vol. 13, 2463, 2023.

[3] Chiu, C.K., Lays, D.P., Ricky, and Krasna, W.A., "Anchorage strength development of headed bars in HSRC external beam-column joints considering side-face blowout failure under monotonic loading", Engineering Structures, Vol. 239, 112218, pp. 1-15, 2021.

[4] Santos, J.P.B., Oliveira, M.H., Lima, N.W.B., Filho, M.J.M.P., and Ferreira, M.P., "A parametric finite element study of concrete cone failure in headed bars under tensile loading", Lat. Am. j. solids struct, Vol. 21, 2, 2024.

[5] H. Mohsuni, T. Matsui, Y. Sanada, J. Sakuta, T. Kiyohara, Y. Kim and T. Adachi, "Pullout Tests on Concrete Breakout Strength of Headed Reinforcement Bars Embedded in Roof Exterior Beam-Column Joints," Journal of Advanced Concrete Technology, Vol. 21, pp.392-404, 2023.

[6] ITOCHU Techno-Solutions Corporation: FINAL HELP, 2018.

[7] Naganuma K., "Stress-Strain Relationship for Concrete under Tri-axial Compression", Journal of Structural and Construction Engineering (Transactions of AIJ), No.474, pp.163-170, 1995.

[8] Nakamura H., Higai T., "Compressive Fracture Energy and Fracture Zone Length of Concrete, Seminar on Post-peak Behavior of RC Structures Subjected to Seismic Load", JCI-C51E, Vol.2, pp. 259-272, 1999.

[9] Izumo J., Shima H., Okamura, H., "Analytical Model for Reinforced Concrete Panel Elements Subjected to In-Plane Forces", Concrete Journal, No. 87.9-1, pp.107-120, 1987.

[10] Vecchio, F.J., and Collins, M.P., "The Modified Compression-Field Theory for Reinforced Concrete Elements Subjected to Shear", ACI Journal, Vol.83, No.2, pp.219-231,1986.

[11] Naganuma, K., "Study on nonlinear analysis method for reinforced concrete wall structures (Part 1), Architectural Institute of Japan", Structural Engineering Papers, No. 421, pp. 39-48, 1991.

[12] Walraven, J., (editor), "fib Model Code for Concrete Structures 2010", ISBN: 978-3-433-03061-5, 2013.